

BiGain: Unified Token Compression for Joint Generation and Classification

Jiacheng Liu^{1,*}, Shengkun Tang^{1,*}, Jiacheng Cui¹, Dongkuan Xu², Zhiqiang Shen^{1†}

¹VILA Lab, MBZUAI ²North Carolina State University

Code: <https://github.com/Greenoso/BiGain>

Abstract

Acceleration methods for diffusion models (e.g., token merging or downsampling) typically optimize for synthesis quality under reduced compute, yet they often ignore the model’s latent discriminative capacity. We revisit token compression with a joint objective and present **BiGain**, a training-free, plug-and-play framework that preserves generation quality while markedly improving classification in accelerated diffusion models. Our key insight is frequency separation: mapping feature-space signals into a frequency-aware representation disentangles fine detail from global semantics, enabling compression that respects both generative fidelity and discriminative utility. **BiGain** reflects this principle with two frequency-aware operators: (1) Laplacian-gated token merging, which encourages merges among spectrally smooth tokens while discouraging merges of high-contrast tokens, thereby retaining edges and textures; and (2) Interpolate-Extrapolate KV Downsampling, which downsamples keys/values via a controllable interextrapolation between nearest and average pooling while keeping queries intact, thereby conserving attention precision without retraining. Across DiT- and U-Net-based backbones and multiple datasets of ImageNet-1K, ImageNet-100, Oxford-IIIT Pets, and COCO-2017, our proposed operators consistently improve the speed-accuracy trade-off for diffusion-based classification, while maintaining, sometimes even enhancing generation quality under comparable acceleration. For instance, on ImageNet-1K, with 70% token merging ratio on Stable Diffusion 2.0, BiGain increases classification accuracy by 7.15% while also improving FID for generation by 0.34 (1.85%). Our comprehensive analyses indicate that balanced spectral retention, preserving high-frequency detail alongside low/mid-frequency semantic content is a reliable design rule for token compression in diffusion models. To our knowledge, BiGain is the first framework to jointly study and advance both generation and classification under accelerated diffusion, supporting lower-cost deployment of dual-purpose generative systems.

[†]Corresponding author.

*Equal contribution.

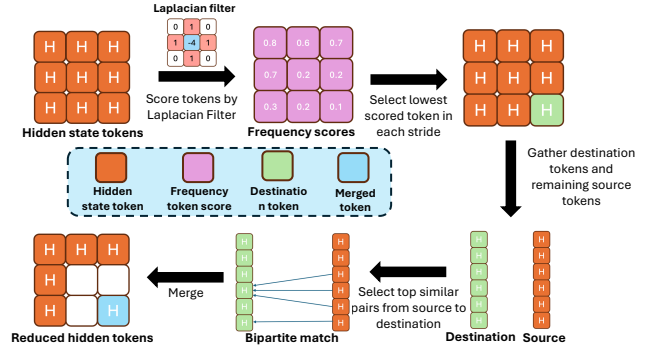


Figure 1. Framework of our **BiGain**TM method. A Laplacian filter is applied to hidden-state tokens to compute local frequency scores. In each spatial stride, the lowest-scoring token is selected as a destination token, while the others form the source set. Destination and source tokens are gathered globally, and a bipartite matching selects top source-destination pairs.

1. Introduction

Diffusion models [12, 21, 27] have become the backbone of modern generative systems, yet their computational footprint during sampling has motivated a surge of training-free acceleration techniques such as token merging [4] and token downsampling [26]. Nearly all of these methods are evaluated primarily for generation/synthesis fidelity under reduced compute (e.g., keeping FID or perceptual quality stable while cutting FLOPs). This single-objective perspective overlooks an increasingly important use case: the same diffusion backbones are potentially and routinely repurposed for downstream recognition, either through linear probes on intermediate features, feature distillation into smaller classifiers [16, 29], or diffusion-based classification protocols [7, 13]. In practice, we observe that accelerations that barely hurt generation can dramatically weaken discriminative performance. This issue is critical as a single diffusion backbone can support both generation and classification through label-conditioned denoising likelihoods.

Joint usage of generation and classification has been utilized across several application domains. In medical imaging, class-conditional diffusion models are used for both diagnostic prediction and counterfactual or uncertainty-aware

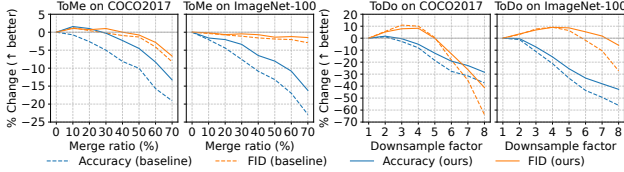


Figure 2. Impact of token compression on diffusion models as our motivation on COCO2017 and ImageNet-100. **Left:** ToMe [4] (baseline) vs. Laplacian-Gated Merge (ours) as the merge ratio increases. **Right:** ToDo [26] (baseline) vs. Interpolate-Extrapolate KV-Downsampling (ours) as the downsample factor grows. Curves report percent change relative to the uncompressed model (\uparrow better; for FID we plot $-\Delta\text{FID}\%$). **Blue:** classification accuracy. **Orange:** generation quality (FID).

reconstruction within one generative prior [9]. In safety-critical perception, robust diffusion classifiers employ the same denoiser for likelihood-based classification and image generation [6]. In industrial visual inspection, diffusion backbones support defect identification and defect reconstruction using the same model [2, 11]. In remote sensing, diffusion models are applied to cloud-removal or super-resolution synthesis while also improving land-cover and object classification [28].

Across these settings, generative and discriminative behaviors arise from one backbone, motivating that token compression methods need to preserve *both* capabilities rather than optimizing solely for synthesis. Therefore, we argue that token compression should be rethought as a joint optimization problem that simultaneously safeguards generative fidelity and discriminative utility. Empirically, naive compression tends to remove precisely those structures that recognition benefits from (edge/texture cues, small objects, high-contrast boundaries), even when global appearance, and thus visual content remains complete. This creates a gap between what “looks good” and what “classifies well”. To bridge this gap, we seek a compression principle that respects the complementary spectral needs of the two capabilities instead of privileging only synthesis. As shown in Fig. 2, baseline compression harms classification accuracy earlier and more sharply than synthesis, sometimes collapsing at extreme sparsity (e.g., COCO2017), whereas our approach consistently mitigates the accuracy drop while keeping generation competitive.

To reflect this, our key insight is frequency separation. Mapping signals of intermediate features into a frequency-aware representation disentangles high-frequency detail (edges, fine textures) from low-mid frequency content (shapes, layouts, semantics). This view yields a simple design rule: balanced spectral retention to preserve the high-frequency components that anchor recognition while maintaining the low-mid bands that support coherent generation. Guided by this principle, compression can prune redundancy without disproportionately harming either side.

In this work, we propose **BiGain**, a training-free, plug-and-play framework composed of two operators. The first, *Laplacian-gated token merging*, computes local Laplacian magnitudes to guide merging: it encourages merges among spectrally smooth tokens and discourages merges of detail-carrying high-contrast tokens. This helps to retain edges and textured micro-structures that classifiers rely on, yet still collapses redundant flat regions to save compute. Crucially, the operator is architecture-agnostic and can be inserted at inference time without retraining. Second, *Interpolate-Extrapolate KV-downsampling* targets attention compute by downsampling keys/values with a controllable interpolation/extrapolation between nearest-neighbor and average pooling (IE-KVD), while leaving queries intact. Keeping queries at full resolution preserves the model’s ability to localize and attend precisely, whereas the KV shrinkage reduces memory and FLOPs smoothly, allowing a tunable speed-accuracy trade-off. Both methods are designed around the same principle of balanced spectral retention: preserving high-frequency detail while maintaining low and mid-frequency semantic content, enabling compression that respects both tasks.

Across DiT- and U-Net-based backbones and multiple datasets, BiGain consistently improves the speed-accuracy trade-off for diffusion-based classification while maintaining generation quality under comparable acceleration, often matching or slightly surpassing the synthesis fidelity of prior accelerations that do not consider recognition at all. Ablations confirm the necessity of frequency awareness: removing Laplacian gating disproportionately hurts classification, and downsampling KV in the frequency balance way is helpful for generation. These results suggest that respecting a balanced spectrum is a robust guiding principle for token compression.

Our contributions of this work are:

- **BiGain** reframes token compression for diffusion models as a bi-objective problem and offers a practical, training-free solution.
- To our knowledge, it is the first framework to jointly study and advance both generation and classification under acceleration of diffusion models.
- Beyond throughput and recognition gains, our study provides practical design guidance in a frequency-aware regime, merges where signals are smooth, downsamples K, V while preserving Q that informs future compression for deployable, dual-purpose generative models.

2. Related Work

Acceleration of Diffusion Models. The iterative nature of diffusion models has spurred methods that reduce the *number of steps* rather than alter the backbone. DDIM [27] introduces non-Markovian sampling to take larger steps, and high-order solvers such as DPM-Solver [15] further

shrink function evaluations while preserving fidelity. Progressive Distillation [24] compresses a teacher into a student that matches quality with fewer steps. These techniques largely treat the denoiser architecture as fixed and are thus orthogonal to our approach, which targets *intra-step* compute via token compression. Meanwhile, pruning for diffusion [5, 8, 32] has also been explored. For example, Diff-Pruning [8] uses a Taylor expansion over pruned timesteps, discarding non-contributory steps and aggregating informative gradients to rank important weights. DiP-GO [32] casts pruning as subnet search: it builds a SuperNet with backup connections over similar features and trains a plug-in pruner with tailored losses to identify redundant computation.

Token Reduction for Diffusion. Token reduction addresses the quadratic cost of attention by removing or merging redundant tokens. TokenLearner [23] learns a small set of summary tokens, while training-free strategies like ToMe [4] greedily merge similar tokens with minimal accuracy loss. Recent works adapt these ideas to diffusion backbones: ToMeSD [3] merges U-Net tokens at inference to accelerate Stable Diffusion, and complementary efforts explore structured pruning/sparsity for Diffusion Transformers [10, 32]. Prior art primarily optimizes *generation* speed-quality trade-offs and typically evaluates synthesis metrics; our method is also training-free and drop-in, but is explicitly designed to preserve generative fidelity *and* discriminative utility through frequency-aware compression.

Diffusion as a Discriminative Learner, and the Open Gap. Beyond synthesis, diffusion models provide strong features for recognition [7, 13]. Diffusion-classifier frameworks use a pre-trained denoiser for per-class scoring or for feature extraction with a lightweight head, yielding competitive image classification [6, 22]. However, the interaction between *token reduction* and *discriminative performance* has been largely overlooked: accelerations that barely hurt synthesis can severely degrade classification. Our work sits at this intersection. We study how token compression affects both capabilities across U-Net/DiT backbones and introduce a frequency-aware, training-free framework that maintains generation quality while markedly improving diffusion-based classification.

3. Methodology

We first revisit token reduction for diffusion models from a *bi-objective* viewpoint: preserve generative fidelity *and* discriminative utility. After reviewing the denoising diffusion setup and the diffusion-classifier decision rule, we formalize shape-preserving token reduction and introduce two training-free, plug-in operators that are *frequency-aware*: (i) Laplacian-gated token merging (L-GTM) and (ii) Interpolate-Extrapolate KV-downsampling (IE-KVD). Both operators avoid cross-timestep caching, which is incom-

patible with diffusion classification, and can be scheduled across timesteps/layers without retraining.

3.1. Preliminaries

A diffusion model [12, 27] specifies the forward process:

$$\begin{aligned} q(\mathbf{x}_t | \mathbf{x}_0) &= \mathcal{N}(\mathbf{x}_t; \sqrt{\bar{\alpha}_t} \mathbf{x}_0, (1 - \bar{\alpha}_t) \mathbf{I}), \\ \mathbf{x}_t &= \sqrt{\bar{\alpha}_t} \mathbf{x}_0 + \sqrt{1 - \bar{\alpha}_t} \epsilon, \epsilon \sim \mathcal{N}(\mathbf{0}, \mathbf{I}). \end{aligned} \quad (1)$$

where \mathbf{x}_0 is the real clean data, \mathbf{x}_t is its noisy version at step t , and ϵ is standard Gaussian noise. The scalar $\bar{\alpha}_t = \prod_{i=1}^t \alpha_i$ defines the cumulative noise schedule: a smaller $\bar{\alpha}_t$ means heavier corruption. Thus, each \mathbf{x}_t is a linear combination of the original signal \mathbf{x}_0 and the noise ϵ .

The denoiser ϵ_θ is trained in the noise-prediction parameterization:

$$\epsilon_\theta(\mathbf{x}_t, c, t) \approx \epsilon, \quad \mathcal{L}(\theta) = \mathbb{E}[\|\epsilon - \epsilon_\theta(\mathbf{x}_t, c, t)\|_2^2], \quad (2)$$

where c denotes an optional conditioning variable (e.g., class label or text prompt).

The network ϵ_θ learns to recover the exact Gaussian noise injected in the forward process. This training objective is equivalent to maximizing a variational lower bound (ELBO) on the data likelihood. It provides two core capabilities: (i) *iterative generative sampling* by reversing the noising process, and (ii) *per-class scoring for classification* by checking which conditioning c yields the lowest prediction error.

3.1.1. Diffusion Classifier

Decision rule. Given \mathbf{x} and class set \mathcal{C} , draw a *shared* Monte Carlo set $\mathcal{S}_{\text{MC}} = \{(t_s, \epsilon_s)\}_{s=1}^S$ for all classes. Define:

$$\begin{aligned} \mathbf{x}_{t_s} &= \sqrt{\bar{\alpha}_{t_s}} \mathbf{x} + \sqrt{1 - \bar{\alpha}_{t_s}} \epsilon_s, \\ \ell(\mathbf{x}, c; t_s, \epsilon_s) &= \|\epsilon_s - \epsilon_\theta(\mathbf{x}_{t_s}, c, t_s)\|_2^2. \end{aligned} \quad (3)$$

Here $\bar{\alpha}_{t_s}$ and ϵ_s are as defined in the diffusion setup above, and ϵ_θ is the same denoiser evaluated under class conditioning c . Thus $\ell(\mathbf{x}, c; t_s, \epsilon_s)$ quantifies how well conditioning on c explains the corruption realized at (t_s, ϵ_s) . The class score and prediction are:

$$\hat{L}(\mathbf{x}, c) = \frac{1}{S} \sum_{s=1}^S \ell(\mathbf{x}, c; t_s, \epsilon_s), \hat{y}(\mathbf{x}) = \arg \min_{c \in \mathcal{C}} \hat{L}(\mathbf{x}, c). \quad (4)$$

Sharing (t_s, ϵ_s) across classes yields a paired-difference estimate of the ELBO for $\log p_\theta(\mathbf{x} | c)$ without changing the decision rule.

Adaptive evaluation (staged pruning). For large $|\mathcal{C}|$, uniform evaluation is costly. We therefore allocate computation in N_{stages} rounds with cumulative budgets $(T_1, \dots, T_{N_{\text{stages}}})$ and keep-counts $(K_1, \dots, K_{N_{\text{stages}}})$ (also see Appendix): at stage i , each surviving class accrues evaluations up to T_i , then only the K_i lowest-score

classes are retained for the next stage. This staged pruning discards unlikely classes early and concentrates samples on plausible ones, reducing wall-clock compute while leaving the final decision $\arg \min_c \hat{L}(x, c)$ unchanged.

3.1.2. Attention and Shape-Preserving Token Reduction

Let the denoiser operate on N latent tokens $\mathbf{X} \in \mathbb{R}^{N \times d}$ (rows x_i). A standard self-attention block forms:

$$\begin{aligned} \mathbf{Q} &= \mathbf{X}\mathbf{W}_Q, & \mathbf{K} &= \mathbf{X}\mathbf{W}_K, & \mathbf{V} &= \mathbf{X}\mathbf{W}_V, \\ \text{Attn}(\mathbf{X}) &= \text{softmax}\left(\frac{\mathbf{Q}\mathbf{K}^\top}{\sqrt{d_k}}\right)\mathbf{V}. \end{aligned} \quad (5)$$

To accelerate while keeping the output length N , we use a shape-preserving reduction $\mathbf{M} \in \mathbb{R}^{N' \times N}$ with $N' < N$, and, if queries are reduced, an unmerge operator $\mathbf{U} \in \mathbb{R}^{N \times N'}$:

$$\mathbf{X} \xrightarrow{\tilde{\mathbf{X}}=\mathbf{M}\mathbf{X}} \tilde{\mathbf{Z}} = F(\tilde{\mathbf{X}}) \xrightarrow{\tilde{\mathbf{X}}=\mathbf{U}\tilde{\mathbf{Z}}} \tilde{\mathbf{X}} \in \mathbb{R}^{N \times d}. \quad (6)$$

We consider two concrete, training-free instances below.

3.2. BiGain: Frequency-Aware Token Compression

Our central design rule is **balanced spectral retention**: preserve high-frequency detail (edges/textures) and low/mid-frequency content (global semantics). We instantiate this via two complementary operators.

3.2.1. Laplacian-Gated Token Merging (L-GTM)

Goal. In this part, we aim to merge spectrally smooth tokens while discouraging merges of high-contrast tokens.

Spectral proxy. We reshape $\mathbf{X} \in \mathbb{R}^{N \times d}$ to $\mathbf{X} \in \mathbb{R}^{H \times W \times C}$ ($C = d$) and compute a per-location frequency magnitude via a spatial Laplacian:

$$\mathbf{F} = \text{Reduce}_c(|\mathbf{X} * \mathbf{L}|), \quad \mathbf{L} = \begin{bmatrix} 0 & 1 & 0 \\ 1 & -4 & 1 \\ 0 & 1 & 0 \end{bmatrix}, \quad \mathbf{F} \in \mathbb{R}^{H \times W}. \quad (7)$$

Here Reduce_c is channel-wise aggregation (e.g., mean or ℓ_2). \mathbf{L} denotes the *Laplacian kernel*, a finite approximation of the second-order derivatives of features in the spatial dimensions (height and width). It is used to measure the degree of difference with respect to the local neighborhood.

Gated merging. Let $s_{ij} = F_{ij}$, in each grid, we take the tokens with the lowest s_{ij} values as the destination set \mathcal{A} (low-frequency anchors), and all remaining tokens as the source set \mathcal{B} . We then merge the top $r\%$ most similar source-destination pairs by equal-weight averaging. The resulting anchors form the reduced sequence $\tilde{\mathbf{X}}$, which defines the merge operator \mathbf{M} ; if needed, \mathbf{U} restores shape by broadcasting averaged values back to removed indices. This encourages compression among spectrally smooth tokens while leaving high-frequency tokens largely intact.

Compute. When \mathbf{M} reduces $\mathbf{Q}, \mathbf{K}, \mathbf{V}$ to N' tokens, attention costs shrink from $\mathcal{O}(N^2d)$ to $\mathcal{O}(N'^2d)$. L-GTM is architecture-agnostic and training-free, we never touch class tokens in DiT nor time/text conditioning tokens in U-Net cross-attention.

Blockwise ABM (Adaptive Block Merging): a fast variant. For additional efficiency, we introduce a tiled variant that pools an $s \times s$ block t only if $\phi(t) = \max_{(i,j) \in t} F_{ij} < \tau$ (with τ as a quantile of \mathbf{F}). Pooled tokens are averaged, others are kept verbatim. ABM is a drop-in replacement for L-GTM in high-resolution stages.

3.2.2. Interpolate–Extrapolate KV-Downsampling (IE-KVD)

Goal. In this component, we aim to reduce attention cost by downsampling keys/values while keeping queries intact to preserve localization and alignment.

Operator. Given a stride s and reduced grid $\tilde{H} \times \tilde{W}$ ($\tilde{N} = \tilde{H}\tilde{W} \ll N$), we define a per-site interpolator/extrapolator between nearest and average pooling:

$$\mathcal{D}_{\alpha,s}(\mathbf{Z})[i] = \alpha \mathbf{Z}[\text{nearest}(i)] + (1-\alpha) \frac{1}{|\mathcal{N}_s(i)|} \sum_{j \in \mathcal{N}_s(i)} \mathbf{Z}[j], \quad (8)$$

We set $\tilde{\mathbf{K}} = \mathcal{D}_{\alpha,s}(\mathbf{K})$ and $\tilde{\mathbf{V}} = \mathcal{D}_{\alpha,s}(\mathbf{V})$, while \mathbf{Q} remains full-resolution. The attention then costs $\mathcal{O}(N\tilde{N}d)$ and preserves output length N .

Preserving \mathbf{Q} maintains fine-grained receptive fields for every output token, which stabilizes synthesis, and critically retains discriminative cues (edge/texture) in diffusion classification, where per-token attention precision matters for the MC scoring rule.

3.3. Compatibility with Diffusion Classification

Our operators are *timestep-local*, deterministic given \mathbf{X} , and do not rely on cross-timestep caches. They therefore integrate seamlessly with the diffusion-classifier decision rule in Sec. 3.1.1: all classes receive identical (t_s, ϵ_s) and identical compression schedules, so the paired-difference estimator remains valid. In practice, we reduce per-class FLOPs and improve accuracy relative to baselines that focus solely on synthesis quality.

4. Experiments

4.1. Experimental Setup

Models. We test our **BiGain** on two representative diffusion models: **Stable Diffusion v2.0** [21] (UNet-based latent diffusion with text conditioning) and **DiT-XL/2** [19] (Transformer backbone), using official pretrained weights. Diffusion classifiers require a noise predictor $\hat{\epsilon}_\theta(x_t, t)$.

Datasets and Metrics. For the classification task, we evaluate on four representative datasets: ImageNet-1K [22],

ImageNet-100 [30], Oxford-IIIT Pets [17], and COCO2017 [14]. Following [13], we evaluate on a 2,000-image validation subset for ImageNet-1K (linear cost in $|\mathcal{C}|$), full validation splits are used elsewhere. We report Top-1 accuracy for single-label datasets and Top-1 precision plus mAP (macro) for multi-label COCO. For generation we evaluate on COCO2017 captions, ImageNet-100, and ImageNet-1K, reporting FID metric. DiT-XL/2 is evaluated only on ImageNet datasets (class-index conditioning, no free-form prompts), while Stable Diffusion v2.0 is evaluated on all datasets using text class prompts. Efficiency is reported as sparsity and FLOPs (both total and attention FLOPs). More details are provided in our appendix.

Implementation Details. Considering the unified timestep policy, also to make generation and diffusion-classifier settings directly comparable, we apply the same token-reduction policy at every denoising step t . We do not cache merged pairings or pooling indices across timesteps, all reductions are recomputed per step and per block. This avoids t -dependent artifacts for synthesis and, because the diffusion classifier is a Monte-Carlo estimator over (t, ϵ) , keeps the schedule temporally consistent, reducing variance.

4.2. Comparisons to State-of-the-Art Approaches

Table 1 presents the comparisons with state-of-the-art approaches on Oxford-IIIT Pets using Top-1 accuracy under $\sim 10\%$ FLOPs reduction. The no-acceleration baseline is 81.03%. Token-merging/pruning baselines suffer large drops: ToMe (8.07%) and SiTo (12.19%), with pruning methods DiP-GO (4.50%) and MosaicDiff (3.65%), showing that compression tuned for synthesis often harms recognition. Our Laplacian-gated merging (**BiGain_{TM}**) retains far more accuracy (78.38%, 2.65% drop), cutting the loss by 27~78% vs. these methods at matched FLOPs. In the downsampling regime (14.2% FLOPs), ToDo slightly decreases the accuracy (-1.88%), while our Interpolate-Extrapolate KV-downsampling (**BiGain_{TD}**) is the best overall (79.90%, only 1.13% drop), also with much better generation ability than ToDo, as we will discuss later. Overall, **BiGain** delivers the strongest classification under comparable compute.

4.3. Classification vs. Generation

We provide classification and generation comparisons under *Token Downsampling* in Table 2 (SD-2.0 backbone) and Table 3 (DiT-XL/2). As shown, our method consistently outperforms the baseline, and the advantage becomes more pronounced as the downsampling ratio increases. The same trend holds for generation: with higher downsampling factors, our approach yields increasingly better results. We further observe (Table 3) that the ToDo method performs very poorly on the DiT-XL/2 model, whereas our method remains more stable on this backbone. Furthermore, with



Figure 3. Qualitative comparison of BiGain_{TM} and ToMe on SD-2.0 backbone. From left to right: BiGain_{TM} with 70%, 50%, and 30% merge ratios, no acceleration, then ToMe with 30%, 50%, and 70% merge ratios.



Figure 4. Qualitative comparison of BiGain_{TD} and ToDo on SD-2.0 backbone. From left to right: BiGain_{TD} with downsampling factors $4\times$, $3\times$, and $2\times$, no acceleration, then ToDo with factors $2\times$, $3\times$, and $4\times$.

relatively small downsampling ($2\times$), our method can match or slightly surpass the original unaccelerated model in both classification and generation (see Fig. 4 for a qualitative comparison in generation task).

For *Token Merging*, classification and generation comparisons are provided in Table 4 (SD-2.0 backbone) and Table 5 (DiT-XL/2). The results mirror those under downsampling: as the merging ratio increases (i.e., with more aggressive pruning), our method achieves substantially better performance than the baseline. In particular, our classification accuracy significantly surpasses ToMe, while our generation capability also exceeds it (see Fig. 3 for a qualitative comparison). These results highlight the dual advantages of our approach in both classification and generation.

4.4. Ablation

Where to reduce¹. As shown in Table 6, we compare applying token reduction to *self-attention only* (SA), *self+cross attentions* (SA+CA), and *self+cross+MLP* (SA+CA+MLP). We find that **SA-only** consistently delivers the best quality-efficiency trade-off: it preserves prompt adherence (avoiding CA degradation) and avoids compounding bias through MLP compression. On Pets, SA-only attains the highest accuracy, while SA+MLP reduces prompt fidelity and SA+CA+MLP further harms fine details. *Conclusion:* we adopt **SA-only** reduction as default for all SD 2.0 experiments.

How to score tokens. As shown in Table 8, local frequency cues dominate: Laplacian Filter (ℓ_1) is best at all

¹Unless noted otherwise, ablations are conducted on Oxford-IIIT Pets with identical sampling schedules, classifier settings (for classification ablations), and reduction ratios as in the main results.

Table 1. Classification accuracy (Acc@1) on Pets dataset under similar FLOPs reduction.

Method	Acceleration Type	FLOPs Reduction \uparrow	Acc@1 \uparrow (%)	Δ vs. Baseline \downarrow
Baseline (No Accel.)	None	–	81.03	–
ToMe [4]	Token Merging/Pruning	10%	72.96	\downarrow 8.07
DiP-GO [32]	Model Pruning	10%	76.53	\downarrow 4.50
SiTo [31]	Token Merging/Pruning	7%	68.84	\downarrow 12.19
MosaicDiff [10]	Model Pruning	10%	77.38	\downarrow 3.65
BiGain_{TM} (Ours)	Token Merging/Pruning	10%	78.38	\downarrow 2.65
ToDo [26]	Token Downsampling	14.2%	79.15	\downarrow 1.88
BiGain_{TD} (Ours)	Token Downsampling	14.2%	79.90	\downarrow 1.13

Table 2. SD-2.0 **Token Downsampling**: Classification (Acc@1 on Pets, ImageNet-100; Acc@1 and mAP on COCO-2017) and generation fidelity (FID \downarrow) vs. downsampling factor. For classification, we fix the interextrapolation factor at 0.9 across all timesteps to ensure stability. For generation, we linearly vary the factor from 0.8 (early steps) to 1.2 (later steps), shifting emphasis from low- to high-frequency information. Gray color indicates the same generation results as the above group.

Method	No Accel.	Classification \uparrow (TD \times)								No Accel.	Generation \downarrow (TD \times)		
		2 \times	3 \times	4 \times	5 \times	6 \times	7 \times	8 \times	2 \times		3 \times	4 \times	
Pets													
Avg-pooling (baseline)		77.02	73.45	71.26	69.00	67.56	66.66	65.13		38.50	39.42	39.74	
ToDo [26]	81.03	81.30	79.15	77.46	72.74	66.74	62.87	56.16	35.01	33.52	32.38	31.48	
BiGain_{TD} (Ours)		81.52	79.91	78.03	74.92	70.86	69.33	66.03		32.19	30.44	29.21	
$\Delta \uparrow$		\uparrow 0.22	\uparrow 0.76	\uparrow 0.57	\uparrow 2.18	\uparrow 4.12	\uparrow 6.46	\uparrow 9.87		\downarrow 1.33	\downarrow 1.94	\downarrow 2.27	
ImageNet-100													
Avg-pooling (baseline)		58.50	49.52	45.54	40.96	38.74	38.12	37.40		19.31	23.08	26.59	
ToDo [26]	73.12	72.30	64.96	57.62	48.70	41.22	37.04	32.12	17.64	16.86	15.93	15.63	
BiGain_{TD} (Ours)		72.88	67.78	61.72	54.48	48.78	45.30	41.90		16.46	15.46	15.46	
$\Delta \uparrow$		\uparrow 0.58	\uparrow 2.82	\uparrow 4.10	\uparrow 5.78	\uparrow 7.56	\uparrow 8.26	\uparrow 9.78		\downarrow 0.40	\downarrow 0.47	\downarrow 0.17	
COCO-2017													
Acc@1 Avg-pooling (baseline)		62.98	55.94	52.46	48.74	46.88	47.38	46.74		30.52	35.92	41.23	
Acc@1 ToDo [26]	70.84	71.66	68.90	65.16	57.70	51.26	48.52	44.40	26.79	25.26	23.86	24.10	
Acc@1 BiGain_{TD} (Ours)		72.04	70.52	67.28	61.98	57.26	54.66	50.72		24.29	23.17	24.05	
$\Delta \uparrow$		\uparrow 0.38	\uparrow 1.62	\uparrow 2.12	\uparrow 4.28	\uparrow 6.00	\uparrow 6.14	\uparrow 6.32		\downarrow 0.97	\downarrow 0.69	\downarrow 0.05	
mAP Avg-pooling (baseline)		44.25	40.96	38.98	36.89	35.77	35.79	35.38		30.52	35.92	41.23	
mAP ToDo [26]	46.01	46.59	45.56	44.07	40.31	36.95	35.50	33.34	26.79	25.26	23.86	24.10	
mAP BiGain_{TD} (Ours)		46.97	46.28	44.81	42.54	40.28	38.82	36.93		24.29	23.17	24.05	
$\Delta \uparrow$		\uparrow 0.38	\uparrow 0.72	\uparrow 0.74	\uparrow 2.23	\uparrow 3.33	\uparrow 3.32	\uparrow 3.59		\downarrow 0.97	\downarrow 0.69	\downarrow 0.05	

Table 3. DiT-XL/2 **Token Downsampling**: Classification (Acc@1) and generation fidelity (FID \downarrow) vs. downsampling factor. For both classification and generation, we fix the interpolate-extrapolate factor at 0.1 across all timesteps. TD Factor: Token Downsampling factor.

Method	No Accel.	Classification \uparrow (TD \times)					No Accel.	Generation \downarrow (TD \times)				
		2 \times	3 \times	4 \times	5 \times	2 \times		3 \times	4 \times	5 \times		
ImageNet-100												
Avg-pooling (baseline)		78.34	61.04	48.40	33.26		40.13	33.57	30.25	41.61		
ToDo [26]	84.82	69.34	8.46	4.74	3.32	47.53	40.48	190.18	206.52	215.04		
BiGain_{TD} (Ours)		78.42	61.58	48.72	34.00		40.13	32.95	29.87	40.55		
$\Delta \uparrow$		\uparrow 9.08	\uparrow 53.12	\uparrow 43.98	\uparrow 30.68		\downarrow 0.35	\downarrow 157.23	\downarrow 176.65	\downarrow 174.49		

merge ratios, outperforming global statistics (norms, channel variance), spectral DFT measures, and cosine similarity by 0.3~1.9%. This supports our frequency-aware design and motivates using a Laplacian proxy for gated merging. Overall, for SD-2.0, token merging in SA with Laplacian scoring provides the strongest quality-efficiency trade-off under our ablation protocol. The detailed mathematical for-

mulations of these score heuristics can be seen in supplementary material.

4.5. Analysis

Further Speedup. *Our vanilla Laplacian Merge.* Before the Q/K/V projections, we run a 2-D Laplacian filter on the hidden map to score each token by local frequency (con-

Table 4. SD-2.0 **Token Merging**: Classification (Acc@1 on Pets, ImageNet-100/1K; Acc@1 and mAP on COCO-2017) and generation fidelity (FID ↓) vs. Token Merging Ratio.

Method	No Accel.	Classification ↑ (Token Merging Ratio)							No Accel.	Generation ↓ (Token Merging Ratio)						
		10%	20%	30%	40%	50%	60%	70%		10%	20%	30%	40%	50%	60%	70%
Pets																
ToMe		80.10	79.88	78.44	76.42	72.96	69.93	65.76		35.05	35.30	35.71	36.26	37.00	37.63	38.35
BiGain_{TM} (Ours)	81.03	81.16	81.16	80.40	80.07	78.38	76.04	74.63	35.01	35.00	35.12	35.01	35.99	36.52	36.99	37.73
Δ ↑		↑1.06	↑1.28	↑1.96	↑3.65	↑5.42	↑6.11	↑8.87		↓0.05	↓0.18	↓0.70	↓0.27	↓0.48	↓0.64	↓0.62
ImageNet-100																
ToMe		71.60	69.90	67.58	65.18	63.48	60.70	56.38		41.51	41.68	41.82	42.02	42.15	42.21	42.58
BiGain_{TM} (Ours)	73.12	71.94	71.62	70.64	68.38	67.24	65.20	61.28	41.37	41.43	41.64	41.55	41.65	41.93	41.86	41.98
Δ ↑		↑0.34	↑1.72	↑3.06	↑3.20	↑3.76	↑4.50	↑4.90		↓0.08	↓0.04	↓0.27	↓0.37	↓0.22	↓0.35	↓0.60
ImageNet-1K																
ToMe		55.50	54.25	52.35	50.65	47.55	43.55	37.35		17.57	17.66	17.74	17.74	17.83	17.97	18.42
BiGain_{TM} (Ours)	57.05	57.25	56.50	55.80	54.80	52.50	49.10	44.50	17.64	17.54	17.48	17.52	17.53	17.58	17.69	18.08
Δ ↑		↑1.75	↑2.25	↑3.45	↑4.15	↑4.95	↑5.55	↑7.15		↓0.03	↓0.18	↓0.22	↓0.21	↓0.25	↓0.28	↓0.34
COCO-2017																
Acc@1 ToMe		70.32	68.98	67.3	65.08	63.72	59.72	57.32		26.45	26.68	26.85	27.04	27.15	27.89	29.00
Acc@1 BiGain_{TM}	70.84	71.96	71.56	70.64	69.20	67.64	64.94	61.44	26.79	26.51	26.60	26.52	26.79	27.00	27.55	28.57
Δ ↑		↑1.64	↑2.58	↑3.34	↑4.12	↑3.92	↑5.22	↑4.12		↑0.06	↓0.08	↓0.33	↓0.25	↓0.15	↓0.34	↓0.43
mAP ToMe		46.04	45.35	44.50	43.43	42.82	41.01	40.07		26.45	26.68	26.85	27.04	27.15	27.89	29.00
mAP BiGain_{TM}	46.01	46.38	46.21	46.05	45.50	44.94	43.98	42.44	26.79	26.51	26.60	26.52	26.79	27.00	27.55	28.57
Δ ↑		↑0.34	↑0.86	↑1.55	↑2.07	↑2.12	↑2.97	↑2.37		↑0.06	↓0.08	↓0.33	↓0.25	↓0.15	↓0.34	↓0.43

Table 5. DiT-XL/2 **Token Merging**: Classification (Acc@1) and generation fidelity (FID ↓) vs. Token Merging Ratio.

Method	No Accel.	Classification ↑ (Token Merging Ratio)							No Accel.	Generation ↓ (Token Merging Ratio)						
		10%	20%	30%	40%	50%	60%	70%		10%	20%	30%	40%	50%	60%	70%
ImageNet-100																
ToMe		80.86	78.02	75.3	71.38	68.24	62.06	53.88		41.51	41.68	41.83	42.02	42.15	42.21	42.58
BiGain_{TM}	84.82	83.56	82.2	79.92	77.38	73.68	68.34	61.76	47.53	41.43	41.61	41.56	41.65	41.92	41.77	41.89
Δ ↑		↑2.70	↑4.18	↑4.62	↑6.00	↑5.44	↑6.28	↑7.88		↓0.08	↓0.07	↓0.27	↓0.37	↓0.23	↓0.44	↓0.69

Table 6. **Ablation of token-merging locations in Stable Diffusion 2.0 on Pets**. Self-Attention (SA) is always merged; Cross-Attention (CA) and MLP are toggled. Results reported at merge ratios $r \in \{0.7, 0.5, 0.3\}$. The underlined results indicate the best performance across all configurations.

Method	SA only			SA+CA			SA+MLP			SA+CA+MLP		
	0.7	0.5	0.3	0.7	0.5	0.3	0.7	0.5	0.3	0.7	0.5	0.3
ToMe [4]	65.76	72.96	78.44	61.68	68.41	74.46	51.43	58.71	66.35	50.86	59.53	66.20
BiGain_{TM} (Ours)	74.63	78.38	80.40	73.89	78.03	79.56	68.27	74.93	77.98	68.25	74.84	77.95

trast w.r.t. its four neighbors). We then partition the feature map into $s_x \times s_y$ cells; within each cell, low-frequency tokens serve as *destinations* and the remaining *source* tokens are greedily assigned by cosine similarity. Because merging acts like a low-pass filter that can destroy high-freq detail, we restrict merging to low-freq tokens only. *Two faster variants*. (1) *Our Cached Assignment Merge*: in the highest-resolution U-Net stages (two Transformer blocks for down sampling and three for up sampling), compute the merge/unmerge map once in the first attention block and reuse it within the stage. (2) *Our Adaptive Block Merge*: after computing Laplacian scores, aggregate them per cell and merge entire low-frequency cells with no per-token matching, yielding extra speed with minimal accuracy loss. As shown in Table 7, both variants closely track Laplacian-

Gated Merge across 10~70% merge ratios across different datasets while providing additional FLOPs savings.

Visualization. We compare token-importance maps for generation and classification to reveal their different spectral needs. As in Fig. 5, frequency-aware reduction yields a favorable bias-variance trade-off: retaining low-frequency tokens stabilizes classification, while selectively keeping high-frequency tokens preserves generation quality, making one heuristic effective for both tasks. To illustrate our Laplacian scoring, we probe SD-2.0 at the highest-resolution upsampling block and visualize pre-attention hidden states filtered by a 2-D Laplacian. Maps are averaged over 100 noise draws without a text prompt to reduce variance, to reveal model’s intrinsic frequency sensitivity.

In Fig. 6, we compare ToMe vs. **BiGain_{TM}** at 90% merge

Table 7. Further speedup on SD-2.0 **Token Merging**: classification performance vs. merge ratio. Acc@1 for single-label datasets; Acc@1 and mAP for multi-label COCO-2017. GFLOPs are measured at merge ratio $r = 0.7$.

Dataset	Method	GFLOPs	10%	20%	30%	40%	50%	60%	70%
Pets	Laplacian Gated Merge	704.99	81.16	81.16	80.4	80.07	78.38	76.04	74.63
	Cached Assignment Merge	698.88	80.29	79.97	79.89	79.01	78.11	75.91	74.49
	Adaptive Block Merge	695.08	80.40	80.16	79.99	79.18	77.84	75.96	74.13
ImageNet-100	Laplacian Gated Merge	704.99	71.94	71.62	70.64	68.38	67.24	65.20	61.28
	Cached Assignment Merge	698.88	71.76	71.16	70.44	69.38	67.78	64.56	61.28
	Adaptive Block Merge	695.08	72.58	71.94	70.58	70.52	68.04	65.36	60.98
ImageNet-1K	Laplacian Gated Merge	704.99	57.25	56.50	55.80	54.80	52.50	49.10	44.50
	Cached Assignment Merge	698.88	56.30	56.05	56.05	53.15	52.30	47.90	44.60
	Adaptive Block Merge	695.08	56.95	56.25	56.00	54.60	51.95	48.20	44.85
COCO-2017	Acc@1 Laplacian Gated Merge	704.99	71.96	71.56	70.64	69.2	67.64	64.94	61.44
	Acc@1 Cached Assignment Merge	698.88	71.72	71.40	70.22	70.02	67.94	64.88	60.88
	Acc@1 Adaptive Block Merge	695.08	71.76	71.44	70.28	69.62	67.26	64.70	60.56
	mAP Laplacian Gated Merge	704.99	46.38	46.21	46.05	45.50	44.94	43.98	42.44
	mAP Cached Assignment Merge	698.88	46.30	46.32	45.94	45.96	45.19	43.93	42.41
	mAP Adaptive Block Merge	695.08	46.35	46.41	45.93	45.87	45.12	43.96	42.32

Table 8. **Ablation over token scoring heuristics for Stable Diffusion 2.0.** Top-1 acc. (%) on Pets dataset across merge ratios. Local Laplacian signals outperform global or spectral metrics.

Scoring method	0.7	0.5	0.3
Global mean deviation	72.96	77.84	79.91
ℓ_1 -norm	73.02	77.11	79.86
ℓ_2 -norm	72.72	77.95	79.61
Channel variance	73.04	77.95	79.83
Laplacian Filter ℓ_1	74.63	78.38	80.40
Laplacian Filter ℓ_2	74.24	77.81	79.80
DFT spectral centroid	73.75	77.92	79.10
DFT amplitude	73.10	77.76	79.34
Cosine to neighbors	74.00	78.22	79.56
Cosine to global mean	73.32	77.84	79.83

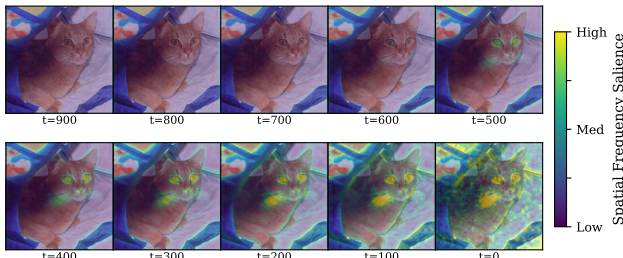


Figure 5. Visualization of our Laplacian-based frequency heuristic on hidden representations from Stable Diffusion-2.0. We probe U-Net at the highest-resolution upsampling stage. The visualization is computed from a noised image without a text prompt, showing the model’s intrinsic frequency-aware reconstruction dynamics. To reduce variance, we randomly sample 100 independent noise realizations and visualize the averaged token saliency map.

on the highest-resolution U-Net transformer layer at $t = 200$ (grayscale = merged). Laplacian-gated merging preserves



Figure 6. **Comparison of token merging schemes.** Left: ToMe [4]; Right: Our BiGain_{TM}. Merging is applied with a merge ratio 90% at the highest-resolution latent layer of the U-Net transformer in Stable Diffusion 2.0 at denoising step $t = 200$. Grayscale indicates merged tokens.

more class-discriminative structure (e.g., the cat’s edges) than standard ToMe.

5. Conclusion

In this work, we revisited token compression for diffusion models as a bi-objective problem, preserving both generative and discriminative abilities, and introduced **BiGain**, a training-free framework built on two frequency-aware operators: *Laplacian-Gated Token Merging* (merge in smooth regions, keep edges) and *Interpolate-Extrapolate KV-Downsampling* (downsample K/V with controllable interextrapolation while keeping Q unchanged). Using DiT/U-Net backbones and multiple datasets, BiGain consistently improves the speed-accuracy trade-off for diffusion-based classification while maintaining, and sometimes even improving generation quality under comparable compute.

Acknowledgements

This work was supported by the MBZUAI–WIS Joint Program for AI Research.

References

- [1] Stephen Batifol, Andreas Blattmann, Frederic Boesel, Saksham Consul, Cyril Diagne, Tim Dockhorn, Jack English, Zion English, Patrick Esser, Sumith Kulal, et al. Flux. 1 kontext: Flow matching for in-context image generation and editing in latent space. *arXiv e-prints*, pages arXiv–2506, 2025. [13](#)
- [2] Farzad Beizaei, Gregory A Lodygensky, Christian Desrosiers, and Jose Dolz. Correcting deviations from normality: A reformulated diffusion model for multi-class unsupervised anomaly detection. In *Proceedings of the Computer Vision and Pattern Recognition Conference*, pages 19088–19097, 2025. [2](#)
- [3] Daniel Bolya and Judy Hoffman. Token merging for fast stable diffusion. In *Proceedings of the IEEE/CVF conference on computer vision and pattern recognition*, pages 4599–4603, 2023. [3](#), [13](#), [16](#)
- [4] Daniel Bolya, Cheng-Yang Fu, Xiaoliang Dai, Peizhao Zhang, Christoph Feichtenhofer, and Judy Hoffman. Token merging: Your vit but faster. In *ICLR*, 2023. [1](#), [2](#), [3](#), [6](#), [7](#), [8](#)
- [5] Thibault Castells, Hyoung-Kyu Song, Bo-Kyeong Kim, and Shinkook Choi. Ld-pruner: Efficient pruning of latent diffusion models using task-agnostic insights. In *Proceedings of the IEEE/CVF Conference on Computer Vision and Pattern Recognition Workshop*, 2024. [3](#)
- [6] Huanran Chen, Yinpeng Dong, Zhengyi Wang, Xiao Yang, Chengqi Duan, Hang Su, and Jun Zhu. Robust classification via a single diffusion model. *arXiv preprint arXiv:2305.15241*, 2023. [2](#), [3](#)
- [7] Kevin Clark and Priyank Jaini. Text-to-image diffusion models are zero shot classifiers. *Advances in Neural Information Processing Systems*, 36:58921–58937, 2023. [1](#), [3](#)
- [8] Gongfan Fang, Xinyin Ma, and Xinchao Wang. Structural pruning for diffusion models. In *Advances in Neural Information Processing Systems*, 2023. [3](#)
- [9] Gian Mario Favero, Parham Saremi, Emily Kaczmarek, Brennan Nichyporuk, and Tal Arbel. Conditional diffusion models are medical image classifiers that provide explainability and uncertainty for free. *arXiv preprint arXiv:2502.03687*, 2025. [2](#)
- [10] Bowei Guo, Shengkun Tang, Cong Zeng, and Zhiqiang Shen. Mosaicdiff: Training-free structural pruning for diffusion model acceleration reflecting pretraining dynamics. In *ICCV*, 2025. [3](#), [6](#)
- [11] Haoyang He, Jiangning Zhang, Hongxu Chen, Xuhai Chen, Zhishan Li, Xu Chen, Yabiao Wang, Chengjie Wang, and Lei Xie. A diffusion-based framework for multi-class anomaly detection. In *Proceedings of the AAAI conference on artificial intelligence*, pages 8472–8480, 2024. [2](#)
- [12] Jonathan Ho, Ajay Jain, and Pieter Abbeel. Denoising diffusion probabilistic models. *Advances in neural information processing systems*, 2020. [1](#), [3](#)
- [13] Alexander C Li, Mihir Prabhudesai, Shivam Duggal, Ellis Brown, and Deepak Pathak. Your diffusion model is secretly a zero-shot classifier. In *Proceedings of the IEEE/CVF International Conference on Computer Vision*, pages 2206–2217, 2023. [1](#), [3](#), [5](#), [11](#), [13](#), [14](#), [15](#)
- [14] Tsung-Yi Lin, Michael Maire, Serge Belongie, James Hays, Pietro Perona, Deva Ramanan, Piotr Dollár, and C Lawrence Zitnick. Microsoft coco: Common objects in context. In *European conference on computer vision*, pages 740–755. Springer, 2014. [5](#), [14](#)
- [15] Cheng Lu, Yuhao Zhou, Fan Bao, Jianfei Chen, Chongxuan Li, and Jun Zhu. Dpm-solver: A fast ode solver for diffusion probabilistic model sampling in around 10 steps. *Advances in neural information processing systems*, 35:5775–5787, 2022. [2](#)
- [16] Benyuan Meng, Qianqian Xu, Zitai Wang, Xiaochun Cao, and Qingming Huang. Not all diffusion model activations have been evaluated as discriminative features. *Advances in Neural Information Processing Systems*, 37:55141–55177, 2024. [1](#)
- [17] Omkar M Parkhi, Andrea Vedaldi, Andrew Zisserman, and CV Jawahar. Cats and dogs. In *2012 IEEE conference on computer vision and pattern recognition*, pages 3498–3505. IEEE, 2012. [5](#), [14](#)
- [18] Adam Paszke, Sam Gross, Francisco Massa, Adam Lerer, James Bradbury, Gregory Chanan, Trevor Killeen, Zeming Lin, Natalia Gimelshein, Luca Antiga, et al. Pytorch: An imperative style, high-performance deep learning library. *Advances in neural information processing systems*, 32, 2019. [14](#)
- [19] William Peebles and Saining Xie. Scalable diffusion models with transformers. *arXiv preprint arXiv:2212.09748*, 2022. [4](#)
- [20] William Peebles and Saining Xie. Scalable diffusion models with transformers. In *Proceedings of the IEEE/CVF international conference on computer vision*, pages 4195–4205, 2023. [14](#)
- [21] Robin Rombach, Andreas Blattmann, Dominik Lorenz, Patrick Esser, and Björn Ommer. High-resolution image synthesis with latent diffusion models. In *Proceedings of the IEEE/CVF conference on computer vision and pattern recognition*, pages 10684–10695, 2022. [1](#), [4](#), [14](#)
- [22] Olga Russakovsky, Jia Deng, Hao Su, Jonathan Krause, Sanjeev Satheesh, Sean Ma, Zhiheng Huang, Andrej Karpathy, Aditya Khosla, Michael Bernstein, et al. Imagenet large scale visual recognition challenge. *International journal of computer vision*, 2015. [3](#), [4](#), [14](#)
- [23] Michael Ryoo, AJ Piergiovanni, Anurag Arnab, Mostafa Dehghani, and Anelia Angelova. Tokenlearner: Adaptive space-time tokenization for videos. *Advances in neural information processing systems*, 34:12786–12797, 2021. [3](#)
- [24] Tim Salimans and Jonathan Ho. Progressive distillation for fast sampling of diffusion models. In *International Conference on Learning Representations*, 2022. [3](#)
- [25] Maximilian Seitzer. pytorch-fid: FID score for PyTorch. *GitHub repository*, 2023. Version 0.3.0. [14](#)

- [26] Ethan Smith, Nayan Saxena, and Aninda Saha. Todo: Token downsampling for efficient generation of high-resolution images. *arXiv preprint arXiv:2402.13573*, 2024. [1](#), [2](#), [6](#), [16](#)
- [27] Jiaming Song, Chenlin Meng, and Stefano Ermon. Denoising diffusion implicit models. *arXiv preprint arXiv:2010.02502*, 2020. [1](#), [2](#), [3](#)
- [28] Tiago Sousa, Benoît Ries, and Nicolas Guelfi. Data augmentation in earth observation: A diffusion model approach. *Information*, 16(2):81, 2025. [2](#)
- [29] Luming Tang, Menglin Jia, Qianqian Wang, Cheng Perng Phoo, and Bharath Hariharan. Emergent correspondence from image diffusion. *Advances in Neural Information Processing Systems*, 36:1363–1389, 2023. [1](#)
- [30] Yonglong Tian, Dilip Krishnan, and Phillip Isola. Contrastive multiview coding. In *European conference on computer vision*, pages 776–794. Springer, 2020. [5](#), [14](#)
- [31] Evelyn Zhang, Jiayi Tang, Xuefei Ning, and Linfeng Zhang. Training-free and hardware-friendly acceleration for diffusion models via similarity-based token pruning. In *Proceedings of the AAAI Conference on Artificial Intelligence*, 2025. [6](#), [16](#)
- [32] Haowei Zhu, Dehua Tang, Ji Liu, Mingjie Lu, Jintu Zheng, Jinzhang Peng, Dong Li, Yu Wang, Fan Jiang, Lu Tian, et al. Dip-go: A diffusion pruner via few-step gradient optimization. *Advances in Neural Information Processing Systems*, 2024. [3](#), [6](#)

Supplementary Material

Contents

A Frequency-Aware Token Reduction and Diffusion Classification	11
A.1 Diffusion Classifier and Paired Difference	11
A.2 Bandwise Decomposition	12
A.3 Token Reduction as a Spectral Operator	12
A.4 A Margin–variance Improvement Criterion	12
A.5 Interpretation and Scope	13
B Implementation Details	13
B.1 Datasets and Evaluation Protocols	13
B.2 Multi-Label Classification Metric	13
B.3 Model Configurations	14
B.4 Token Compression	14
B.5 Efficiency Evaluation	14
C Algorithm	15
C.1 Adaptive Diffusion Classifier	15
C.2 Frequency-Aware Token Scoring	15
C.3 BiGain _{TM}	15
C.4 BiGain _{TD}	16
C.5 Additional Ablations and Results	17
D Use of Large Language Models	18

A. Frequency-Aware Token Reduction and Diffusion Classification

In this section we provide a simple stylized model showing how frequency-aware token reduction can tighten the diffusion-classifier decision, viewed through a margin–variance trade-off on the paired Monte Carlo estimator introduced in Sec. 3.1.1 of the main paper.

A.1. Diffusion Classifier and Paired Difference

Recall the diffusion-classifier score [13]:

$$S(x, c) = \mathbb{E}_{t, \epsilon} \|\epsilon - \epsilon_\theta(x_t, c, t)\|_2^2, \quad (9)$$

$$x_t = \sqrt{\alpha_t} x + \sqrt{1 - \alpha_t} \epsilon.$$

The prediction is $\hat{c}(x) = \arg \min_{c \in \mathcal{C}} S(x, c)$, implemented using *paired sampling*: for a shared Monte Carlo set $\mathcal{S}_{\text{MC}} = \{(t_s, \epsilon_s)\}_{s=1}^{S_{\text{MC}}}$ (reused for all classes as in Sec. 3.1.1) we approximate $S(x, c)$ by

$$\hat{S}_{\text{MC}}(x, c) = \frac{1}{S_{\text{MC}}} \sum_{s=1}^{S_{\text{MC}}} \ell(x, c; t_s, \epsilon_s), \quad (10)$$

$$\ell(x, c; t, \epsilon) = \|\epsilon - \epsilon_\theta(x_t, c, t)\|_2^2.$$

Fix the true class c^* and a distractor \tilde{c} . For one paired draw $(t, \epsilon) \sim p(t)p(\epsilon)$, we define

$$D(t, \epsilon) = \ell(x, \tilde{c}; t, \epsilon) - \ell(x, c^*; t, \epsilon). \quad (11)$$

Let

$$\mu = \mathbb{E}[D], \sigma^2 = \text{Var}[D]. \quad (12)$$

With S_{MC} shared samples we obtain the paired estimator

$$\hat{\Delta}_{\text{MC}} = \frac{1}{S_{\text{MC}}} \sum_{s=1}^{S_{\text{MC}}} D(t_s, \epsilon_s), \quad (13)$$

$$\mathbb{E}[\hat{\Delta}_{\text{MC}}] = \mu, \text{Var}(\hat{\Delta}_{\text{MC}}) = \frac{\sigma^2}{S_{\text{MC}}}.$$

For a consistent classifier we have $\mu > 0$, and misclassification against \tilde{c} corresponds to the tail event $\hat{\Delta}_{\text{MC}} \leq 0$.

By Cantelli’s inequality, for any random variable Z with mean m and variance v , $\Pr(Z - m \leq -a) \leq v/(v + a^2)$ for $a > 0$. Applying this to $Z = \hat{\Delta}_{\text{MC}}$, $m = \mu$, $a = \mu$ yields

$$\Pr(\hat{\Delta}_{\text{MC}} \leq 0) \leq \frac{\sigma^2/S_{\text{MC}}}{\mu^2 + \sigma^2/S_{\text{MC}}} = f(r), r = \frac{\sigma}{\mu}, \quad (14)$$

where $f(r)$ is strictly increasing in r . Thus, tightening the Cantelli bound is equivalent to decreasing the ratio r .

A.2. Bandwise Decomposition

We now introduce a simple frequency-domain model of the paired difference. Let $\{\phi_k\}$ be an orthonormal 2-D DCT/Fourier basis over the spatial token grid. For each (t, ϵ) and class c , we expand the error as:

$$\ell(x, c; t, \epsilon) = \sum_k \omega_k(t) |\widehat{\epsilon}(k) - \widehat{\epsilon}_\theta(k; t, c)|^2, \quad (15)$$

where $\widehat{\cdot}(k)$ denotes the coefficient in band k and $\omega_k(t) \geq 0$ is a per-band reliability weight (e.g., arising from the ELBO weighting over t).

We define the bandwise paired difference as:

$$\Delta_k(t, \epsilon) := |\widehat{\epsilon}(k) - \widehat{\epsilon}_\theta(k; t, \tilde{c})|^2 - |\widehat{\epsilon}(k) - \widehat{\epsilon}_\theta(k; t, c^*)|^2, \quad (16)$$

so that

$$D(t, \epsilon) = \sum_k \omega_k(t) \Delta_k(t, \epsilon). \quad (17)$$

Let

$$\begin{aligned} \mu_k &:= \mathbb{E}_{t, \epsilon}[\Delta_k(t, \epsilon)], \\ \sigma_k^2 &:= \text{Var}_{t, \epsilon}[\Delta_k(t, \epsilon)], \\ w_k &:= \mathbb{E}_t[\omega_k(t)]. \end{aligned} \quad (18)$$

Assuming that cross-band covariances are weak,

$$\text{Cov}(\Delta_i, \Delta_j) \approx 0, \quad i \neq j, \quad (19)$$

we obtain the approximation

$$\begin{aligned} \mu &\approx \sum_k w_k \mu_k, \\ \sigma^2 &\approx \sum_k w_k^2 \sigma_k^2. \end{aligned} \quad (20)$$

Intuitively, discriminative classifiers benefit from high-frequency components (edges and textures) to refine the class margin μ . Coarse structures (low frequencies) provide stable semantic cues, while fine structures (high frequencies) often distinguish specific classes. Consequently, although high-frequency bands may exhibit larger variance under stochastic sampling, they can still carry strong class-specific information for the correct class. A reduction strategy that indiscriminately suppresses these frequencies, effectively acting as a low-pass filter with $H_P(k) \approx 0$ for high k , risks inducing a large margin loss $\Delta\mu$ that can outweigh any variance reduction $\Delta\sigma^2$.

A.3. Token Reduction as a Spectral Operator

We consider an attention block operating on a window of tokens, with pre-reduction features $z_i = s_i + n_i$, where s_i denotes structured signal and n_i zero-mean perturbations. A shape-preserving reduction operator P maps the window

to a reduced representation (e.g., via merging or downsampling). Under a local linearization of the block, and for operators such as IE-KVD that are explicitly linear in each neighborhood, we approximate its effect via a *windowed frequency response* $H_P(k)$:

$$\begin{aligned} \mu' &\approx \sum_k w_k H_P(k) \mu_k, \\ \sigma'^2 &\approx \sum_k w_k^2 H_P(k)^2 \sigma_k^2. \end{aligned} \quad (21)$$

This spectral model provides a useful approximation of how token-reduction operators reshape the band-weighted paired statistic. For strictly linear operators such as IE-KVD the frequency response $H_P(k)$ is exact, while for merging-based operators (e.g., L-GTM, ABM), it serves as a local linearization that captures their dominant low-pass-like behaviour.

In particular, any operator P whose effective response $H_P(k)$ (exact for IE-KVD, approximate for merging) acts as a *bandwise shrinkage rule*, with $H_P(k) \approx 1$ on margin-rich bands and $H_P(k) < 1$ on variance-heavy bands, will tend to reduce the ratio $r = \sigma/\mu$ in equation 14. Both of our proposed modules, Laplacian-gated token merging (L-GTM) and Interpolate–Extrapolate KV-Downsampling (IE-KVD), are designed to approximate this behavior: they selectively smooth or merge tokens that are redundant while retaining tokens that appear informative, producing a frequency-selective shrinkage profile.

For IE-KVD, which is a linear filtered downsampling operator, the spectral interpretation is exact, for merging-based operators, it should be viewed as an approximation under local linearization. We emphasize that this analysis is a stylized model: it relies on linearization and approximate bandwise decorrelation, and is intended to clarify the design principle behind our frequency-aware token reduction rather than to provide a formal guarantee.

A.4. A Margin–variance Improvement Criterion

We define the changes in mean margin and variance as

$$\begin{aligned} \Delta\mu &:= \mu - \mu', \\ \Delta\sigma^2 &:= \sigma^2 - \sigma'^2. \end{aligned} \quad (22)$$

We are interested in when the ratio $r' = \sigma'/\mu'$ is smaller than $r = \sigma/\mu$, since by equation 14 this implies a tighter Cantelli bound.

Theorem 1 (Spectral margin–variance improvement). *Assume $\mu > 0$, $\mu' > 0$, $\sigma^2 > 0$, and that μ' and σ'^2 are defined as above. Then the post-reduction ratio r' is smaller than the original ratio r , $r' < r$, if and only if*

$$\Delta\sigma^2 > 2 \frac{\sigma^2}{\mu} \Delta\mu - \frac{\sigma^2}{\mu^2} (\Delta\mu)^2. \quad (23)$$

Moreover, when $|\Delta\mu| \ll \mu$, the first-order sufficient condition

$$\Delta\sigma^2 > 2 \frac{\sigma^2}{\mu} \Delta\mu \quad (24)$$

guarantees $r' < r$ and hence a strictly improved Cantelli bound.

Proof. Since $\mu > 0$ and $\mu' > 0$ we have $r, r' \geq 0$, so $r' < r$ is equivalent to $r'^2 < r^2$. The condition $r'^2 < r^2$ is equivalent to $\frac{\sigma^2 - \Delta\sigma^2}{(\mu - \Delta\mu)^2} < \frac{\sigma^2}{\mu^2}$. Multiplying both sides by the positive denominators and rearranging gives $\Delta\sigma^2\mu^2 - 2\sigma^2\mu\Delta\mu + \sigma^2(\Delta\mu)^2 > 0$, which after dividing by μ^2 yields equation 23. Expanding the right-hand side of equation 23 to first order in $\Delta\mu/\mu$ gives the sufficient condition equation 24. \square

A.5. Interpretation and Scope

Equation 23, together with the bandwise decompositions of $\Delta\mu$ and $\Delta\sigma^2$, provides a spectral lens for comparing reduction strategies. The term $\Delta\sigma^2 = \sum_k w_k^2(1 - H_P(k)^2)\sigma_k^2$ captures the *variance savings*, while $\Delta\mu = \sum_k w_k(1 - H_P(k))\mu_k$ quantifies the corresponding *margin cost*. Achieving a tighter decision bound ($r' < r$) requires maximizing the former while keeping the latter small.

Standard token-merging approaches (e.g., ToMe [3]) can be interpreted, in our stylized spectral model, as performing spatial averaging: they tend to smooth fine-scale structure and thus resemble a low-pass filter with an effective response $H_P(k) \ll 1$ for high-frequency bands k . Because edges, textures, and other fine-scale structures often yield large μ_k (i.e., high-frequency bands are *margin-rich* for recognition), indiscriminate merging induces a substantial margin loss $\Delta\mu$. If this loss exceeds the allowable threshold in Theorem 1, the classifier’s performance degrades despite any reduction in variance.

In contrast, the proposed **BiGain** is designed to favor this trade-off. Laplacian gating identifies regions where high-frequency content is relatively small, which in our spectral model corresponds to bands with small μ_k . In regions containing significant high-frequency structure (large μ_k), **BiGain** suppresses merging, corresponding to an effective response $H_P(k) \approx 1$ and hence $\Delta\mu \approx 0$ on margin-critical bands in our spectral model. This frequency-aware selection biases the shrinkage profile towards satisfying equation 23, which is consistent with our observation that **BiGain** preserves discriminative utility far better than spectrally agnostic merging schemes.

B. Implementation Details

B.1. Datasets and Evaluation Protocols

B.1.1. Dataset Details

We evaluate on four widely-used benchmarks, summarized in Table 9. Following [13], ImageNet-1K is sub-sampled to 2,000 images for classification to reduce computational cost, while the full validation set is retained for generation experiments.

B.1.2. Diffusion Classifier Protocol

Diffusion-classifier. We follow the *Diffusion Classifier* framework [13], which scores a candidate conditioning c by the expected noise-prediction error $\mathbb{E}_{t,\epsilon}[\|\epsilon - \epsilon_\theta(x_t, c, t)\|_2^2]$ and selects the minimizer. This method is *training-free*, requiring no calibration or finetuning, and enables zero-shot classification directly from pretrained diffusion models. To enable evaluation on large label spaces, we use adaptive evaluation with staged pruning (detailed in Algorithm C.1). We adjust only `TrialList` and `KeepList` based on the size of the candidate set.

For completeness, we also evaluated velocity-prediction flow-matching models (FLUX [1]). Using the `FlowMatchEulerDiscreteScheduler` to construct affine mappings for recovering $\hat{\epsilon}_\theta$ and \hat{x}_0 within DDIM, the released FLUX.1-dev checkpoint performed only marginally better than random guessing under the diffusion-classifier protocol. To avoid adapter-specific confounds and ensure a fair comparison, we restrict all evaluations to standard noise-prediction models.

B.2. Multi-Label Classification Metric

We evaluate performance using mean Average Precision (mAP) for multi-label image classification, computed from a ranked list of labels for each image.

Given an image x with ground-truth label set $\mathcal{Y} \subset \mathcal{C}$, the diffusion classifier assigns each label $c \in \mathcal{C}$ an estimated classification error

$$\hat{L}(x, c) = \frac{1}{S} \sum_{s=1}^S \ell(x, c; t_s, \epsilon_s), \quad (25)$$

where $\ell(x, c; t_s, \epsilon_s)$ and the shared Monte Carlo set $\{(t_s, \epsilon_s)\}_{s=1}^S$ are defined in Sec. 3.1.1 of the main paper. Lower values of $\hat{L}(x, c)$ indicate higher confidence that label c is present.

All labels are ranked in ascending order of $\hat{L}(x, c)$.

Average Precision per image. Let $\{c_1, c_2, \dots\}$ denote the ranked label list. The Average Precision for image x is defined as

$$\text{AP}(x) = \frac{1}{|\mathcal{Y}|} \sum_{k: c_k \in \mathcal{Y}} \frac{|\mathcal{Y} \cap \{c_1, \dots, c_k\}|}{k}, \quad (26)$$

Table 9. Dataset statistics with official splits used in our experiments.

Dataset	Classes	Split	# Images (Cls.)	# Images (Gen.)
ImageNet-100 [30]	100	Val.	5,000	5,000
ImageNet-1K [22]	1,000	Val.	2,000	50,000
Oxford-IIIT Pets [17]	37	Test	3,669	3,669
COCO-2017 [14]	80	Val.	5,000	5,000

Table 10. Adaptive diffusion-classifier parameters per dataset. N_{stages} is the number of pruning stages; `TrialList` is the cumulative number of Monte Carlo trials per candidate by stage; `KeepList` is the number of candidates retained after each stage.

Dataset	N_{stages}	TrialList	KeepList
ImageNet-100	2	[5, 20]	[5, 1]
COCO-2017	2	[5, 20]	[5, 1]
Oxford-IIIT Pets	2	[5, 20]	[5, 1]
ImageNet-1K	3	[5, 20, 100]	[50, 10, 1]

where the sum runs over ranks at which a ground-truth label appears.

Mean Average Precision. The final mAP is obtained by averaging $AP(x)$ over all test images.

B.3. Model Configurations

B.3.1. Prompt Templates

For the classification task, following [13], we use `''a photo of a {class}''` for ImageNet and COCO datasets, and `''a photo of a {class}, a type of pet''` for Oxford-IIIT Pets.

For generation, we use the same templates except for COCO-2017, where we use the official validation captions.

B.3.2. Generation Setup

We standardize generation across both backbones. For Stable Diffusion 2.0 (UNet) [21], we use the EulerDiscreteScheduler with a scaled-linear beta schedule (beta_start 0.00085, beta_end 0.012, 1,000 training steps, epsilon prediction). For DiT-XL/2-512 [20], we use the DDIMScheduler with a linear beta schedule (beta_start 0.0001, beta_end 0.02, 1,000 training steps, epsilon prediction). In both cases, we sample for 50 steps at 512x512 resolution. We apply classifier-free guidance with a scale of 7.5 for Stable Diffusion 2.0 and 4.0 for DiT-XL/2-512. Unless otherwise stated, all experiments are conducted in FP16 precision. For evaluation, FID scores are computed using the `pytorch-fid` implementation [25].

B.4. Token Compression

B.4.1. Compression Settings

Guided by the ablation in Table 6, we apply compression exclusively to self-attention (SA) and leave cross-attention (CA) and MLP blocks intact to preserve prompt adherence. For merging-based operators, merging is performed inside each SA block and an explicit unmerge restores the

original sequence length before the residual addition, ensuring dense outputs for downstream modules. For KV-downsampling operators, only keys and values are subsampled while queries remain full-length, removing the need for unmerge.

Stable Diffusion 2.0 (U-Net). We insert compression exclusively at the highest-resolution encoder layers, where the spatial token count, and thus attention cost is maximal. This targets the primary bottleneck while maintaining quality.

Diffusion Transformer (DiT-XL/2). To assess generality beyond U-Net architectures, we port the same operators to DiT-XL/2. Specifically, token compression is applied within the first 12 transformer blocks, comparing early (blocks 1–6) versus mid-early (blocks 7–12) reduction, while leaving later blocks, where class conditioning and fine structural details consolidate unchanged.

B.4.2. Baseline Implementation

For all token compression baselines, we use the official implementations and default parameters released by the authors, and run them under a common experimental protocol (see Sec. B.1.2 and Sec. B.3.2) to ensure fair comparison and avoid unintentional re-tuning. The only modification we introduce is to vary the token reduction ratio, so that each method can be fairly evaluated under different levels of compression.

B.5. Efficiency Evaluation

To measure the acceleration effect of our token reduction methods, we evaluate on the official Stable Diffusion 2.0 implementation released by Stability AI [21]. All experiments are conducted on a single NVIDIA RTX 4090 GPU in half-precision (`float16`). We report wall-clock sampling time per image batch excluding the VAE encoding/decoding overhead, since our methods target the denoising backbone rather than the autoencoder. FLOPs are measured using `FlopCounterMode` from `torch.utils.flop_counter` [18]. The correspond-

ing runtime and efficiency results are summarized in Table 11, which demonstrates the advantage of our method.

C. Algorithm

C.1. Adaptive Diffusion Classifier

Naïve diffusion classification requires evaluating all candidate classes, and thus its cost grows linearly with the number of classes. To mitigate this, we adopt the adaptive evaluation strategy introduced in the diffusion-classifier framework [13]. At each stage, we allocate a fixed budget of trials across the remaining classes, discard unlikely candidates based on their average error, and retain only the most promising ones. This progressive pruning concentrates computation on high-confidence classes, enabling more fine-grained Monte Carlo error estimation. The procedure is summarized in Algorithm 1.

Algorithm 1 Diffusion Classifier (Adaptive) [13]

Require: test image \mathbf{x} , conditioning inputs $\mathcal{C} = \{\mathbf{c}_i\}_{i=1}^n$ (e.g., text embeddings or class indices), number of stages N_{stages} , list `KeepList` of number of \mathbf{c}_i to keep after each stage, list `TrialList` of number of trials done by each stage

- 1: Initialize `Errors`[\mathbf{c}_i] = list() for each \mathbf{c}_i
- 2: Initialize `PrevTrials` = 0 ▷ How many times we’ve tried each remaining element of \mathcal{C} so far
- 3: **for** stage $i = 1, \dots, N_{\text{stages}}$ **do**
- 4: **for** trial $j = 1, \dots, \text{TrialList}[i] - \text{PrevTrials}$ **do**
- 5: Sample $t \sim [1, 1000]$
- 6: Sample $\epsilon \sim \mathcal{N}(0, I)$
- 7: $\mathbf{x}_t = \sqrt{\alpha_t}\mathbf{x} + \sqrt{1 - \alpha_t}\epsilon$
- 8: **for** conditioning $\mathbf{c}_k \in \mathcal{C}$ **do**
- 9: `Errors`[\mathbf{c}_k].append($\|\epsilon - \epsilon_\theta(\mathbf{x}_t, \mathbf{c}_k, t)\|^2$)
- 10: **end for**
- 11: **end for**
- 12: $\mathcal{C} \leftarrow \underset{S \subset \mathcal{C}; |S|=\text{KeepList}[i]}{\text{argmin}} \sum_{\mathbf{c}_k \in S} \text{mean}(\text{Errors}[\mathbf{c}_k])$ ▷
Keep top `KeepList`[i] conditionings
- 13: `PrevTrials` = `TrialList`[i]
- 14: **end for**
- 15: **return** $\underset{\mathbf{c}_i \in \mathcal{C}}{\text{argminmean}}(\text{Errors}[\mathbf{c}_i])$

C.2. Frequency-Aware Token Scoring

Spectral structure of latent features is important for both discriminative and generative ability. High-frequency tokens encode the information of edges, textures, and small objects, especially at the late denoise stage, which are indispensable for recognition. However, high-frequency tokens can also amplify the variance in the diffusion classifier

since predictions are aggregated over Monte Carlo draws of timesteps and noise; excess high-frequency tokens inflate the per-timestep estimation variance. Moreover, different timesteps emphasize different bands, early denoising focuses on low frequencies (global structure) while later steps emphasize high frequencies (fine detail). Therefore, the compression schedule should be *spectrally balanced and temporally consistent* to avoid injecting avoidable variance across timesteps. The necessity of preserving a balanced spectrum is confirmed empirically in Table 12, where discarding either high- or low-frequency tokens severely harms classification.

Our **BiGain_{TM}** design follows this principle. Since token merging resembles a local low-pass filter, we encourage merging only in small, spectrally smooth neighborhoods, where low-frequency information can be safely aggregated, while protecting detail-rich tokens that anchor class-critical microstructures. This balanced policy removes redundancy without sacrificing classification accuracy or generation fidelity. Practically, we introduce a set of fast, training-free scoring heuristics to decide which tokens to *preserve* (high detail) and which to *merge* (smooth/redundant), and we apply them consistently across timesteps so that each per-timestep classifier score remains reliable and contributes coherently to the Monte Carlo ensemble.

Notation. Let $\mathbf{X} \in \mathbb{R}^{H \times W \times C}$ denote the hidden feature tensor (height H , width W , channels C). For spatial index (i, j) , the token (channel vector) is $\mathbf{x}_{i,j} := \mathbf{X}_{i,j,:} \in \mathbb{R}^C$. The global mean token is $\boldsymbol{\mu} := \frac{1}{HW} \sum_{p=1}^H \sum_{q=1}^W \mathbf{x}_{p,q}$. For a 3×3 spatial kernel \mathbf{L} , $(\mathbf{X} * \mathbf{L})_{i,j,c}$ denotes 2-D convolution at (i, j) on channel c . Let $\mathbb{N}_4(i, j)$ be the (in-bounds) 4-neighborhood of (i, j) (up/down/left/right). The DFT of $\mathbf{x}_{i,j}$ at channel-frequency bin k is $\hat{\mathbf{x}}_{i,j,k} := \sum_{c=1}^C (\mathbf{x}_{i,j})_c e^{-2\pi i (c-1)(k-1)/C}$ for $k \in \{1, \dots, C\}$. We write $\|\cdot\|_p$ for the vector ℓ_p norm, $\|\cdot\| \equiv \|\cdot\|_2$, and $\langle \mathbf{a}, \mathbf{b} \rangle$ for the Euclidean inner product. We compute a scalar score $F_{i,j} \in \mathbb{R}$ per token, where larger values indicate detail-rich tokens and smaller values indicate smooth/redundant tokens. We list all functions of different metrics in Table 13.

For all heuristics except cosine-based ones, larger $F_{i,j}$ indicates stronger local variation and thus high-frequency detail. In contrast, for cosine similarity scores, *smaller* values correspond to tokens that deviate more from their neighbors or the global mean, and are therefore detail-rich.

C.3. BiGain_{TM}

Algorithm 2 presents our frequency-aware token merging method. The core innovation lies in using spectral information to guide merge decisions, ensuring that token reduction preserves both generative fidelity and discriminative utility. The algorithm first applies a frequency scorer \mathcal{F} (default:

Table 11. **Stable Diffusion 2.0 efficiency (batch size 4)**. Wall-clock sampling time per *batch* (seconds) excluding VAE encode/decode. All rows use merge ratio $r = 0.7$.

Method	Time ↓ (s / batch)	Acceleration ↑ (%)	FLOPs ↓ (G)
Baseline (No Accel.)	11.98	–	804.26
SiTo [31]	8.71	27.30	748.49
ToMe [3]	7.37	38.48	704.87
Laplacian Gated Merge (Ours)	7.37	38.48	704.99
Cached Assignment Merge (Ours)	7.29	39.15	698.88
Adaptive Block Merging (Ours)	7.27	39.32	695.08

Table 12. **Classification results on frequency-based KV selection on ImageNet-100**. We compare the standard TODO strategy with frequency-aware variants that select tokens with the highest or lowest Laplacian scores globally. Retaining only high- or low-frequency tokens severely degrades classification performance, highlighting the need to preserve a balanced spectrum.

Downsampling strategy	Acc@1 ↑	KV token sparsity
Todo (Nearest-Neighbor) [26]	72.30	75%
Low-frequency tokens (lowest-laplacian)	45.58	75%
High-frequency tokens (Highest-laplacian)	26.56	75%

Laplacian filtering C.2) to identify local frequency content in the spatial feature map. Tokens with low frequency scores indicate smooth, homogeneous regions amenable to merging, while high scores correspond to edges, textures, and fine details critical for classification.

The destination selection step partitions the spatial layout into regular grids and identifies the lowest-frequency token within each grid as a merge destination. This strategy ensures spatial coverage while directing merging toward spectrally smooth regions. The remaining tokens form a source set, which is then assigned to destinations via bipartite matching based on cosine similarity. By selecting the top- r fraction of most similar pairs, the method preserves semantic coherence while respecting the frequency-based partitioning. After merging and processing through attention layers, an unmerge operation restores the original sequence length for architectural compatibility.

Algorithm 3 presents Adaptive Block Merge (ABM), a computationally efficient variant designed for high-resolution stages where token count is maximal. Rather than per-token assignment, ABM operates at block granularity. After computing frequency scores, the feature map is partitioned into blocks, and blocks are ranked by their frequency content. The lowest-scoring fraction r of blocks are identified as smooth regions and merged via averaging, while high-frequency blocks remain intact. This block-level decision reduces computational complexity of bipartite matching, providing speedup with little accuracy degradation as demonstrated in our Table 7.

C.4. BiGain_{TM}

Algorithm 4 presents our Interpolate-Extrapolate KV-Downsampling method, which reduces attention complex-

Algorithm 2 BiGain_{TM}: Frequency-Aware Token Merging

Require: Tokens $\mathbf{X} \in \mathbb{R}^{N \times d}$, merge ratio r , grid size s , frequency scorer \mathcal{F}

- 1: **function** BIGAINMERGE($\mathbf{X}, r, s, \mathcal{F}$)
- 2: $\mathbf{f} \leftarrow \mathcal{F}(\mathbf{X})$ ▷ Score tokens by frequency content
- 3: $\mathbb{D} \leftarrow \text{SelectDestinations}(\mathbf{f}, s)$ ▷ Lowest frequency per grid
- 4: $\mathbb{S} \leftarrow \{1, \dots, N\} \setminus \mathbb{D}$ ▷ Remaining tokens as sources
- 5: $\mathcal{M} \leftarrow \text{BipartiteMatch}(\mathbf{X}_{\mathbb{S}}, \mathbf{X}_{\mathbb{D}}, r)$ ▷ Similarity-based assignment
- 6: $\mathbf{X}^{\text{merged}} \leftarrow \text{Merge}(\mathbf{X}, \mathcal{M})$ ▷ Combine assigned tokens
- 7: $\mathbf{Z} \leftarrow \text{Process}(\mathbf{X}^{\text{merged}})$ ▷ Apply attention
- 8: **return** Unmerge(\mathbf{Z}, \mathcal{M}) ▷ Restore dimensions
- 9: **end function**

ity by downsampling keys and values while preserving queries at full resolution. This asymmetric approach maintains the model’s ability to attend precisely to all spatial positions while reducing memory and computation. The key innovation is the controllable linear combination of nearest-neighbor and average pooling, allowing fine-grained control over the frequency-preservation trade-off.

Here we use the same interpolate-extrapolate operator $D_{\alpha,s}$ as defined in Eq. 8 of the main paper. This operator blends nearest-neighbor sampling (preserving detail) with average pooling (smoothing), controlled by the parameter $\alpha \in \mathbb{R}$. Keys and values are downsampled as $\hat{K} = D_{\alpha,s}(K)$ and $\hat{V} = D_{\alpha,s}(V)$, while queries remain full resolution.

Table 13. Formulas of different metrics.

Metric Name	Formula
Global mean deviation	$F_{i,j} = \ \mathbf{x}_{i,j} - \boldsymbol{\mu}\ $
ℓ_1 norm	$F_{i,j} = \ \mathbf{x}_{i,j}\ _1$
ℓ_2 norm	$F_{i,j} = \ \mathbf{x}_{i,j}\ $
Channel variance	$F_{i,j} = \frac{1}{C} \sum_{c=1}^C \left((\mathbf{x}_{i,j})_c - \frac{1}{C} \sum_{c'=1}^C (\mathbf{x}_{i,j})_{c'} \right)^2$
Laplacian (ℓ_1)	$F_{i,j} = \frac{1}{C} \sum_{c=1}^C (\mathbf{X} * \mathbf{L})_{i,j,c} , \quad \mathbf{L} = \begin{bmatrix} 0 & 1 & 0 \\ 1 & -4 & 1 \\ 0 & 1 & 0 \end{bmatrix}$
Laplacian (ℓ_2)	$F_{i,j} = \sqrt{\frac{1}{C} \sum_{c=1}^C ((\mathbf{X} * \mathbf{L})_{i,j,c})^2}$
DFT spectral centroid	$F_{i,j} = \frac{\sum_{k=1}^C k \hat{\mathbf{x}}_{i,j,k} }{\sum_{k=1}^C \hat{\mathbf{x}}_{i,j,k} }$
DFT total amplitude	$F_{i,j} = \sum_{k=1}^C \hat{\mathbf{x}}_{i,j,k} $
Cosine similarity to neighbors	$F_{i,j} = \frac{1}{ \mathbb{N}_4(i,j) } \sum_{(p,q) \in \mathbb{N}_4(i,j)} \frac{\langle \mathbf{x}_{i,j}, \mathbf{x}_{p,q} \rangle}{\ \mathbf{x}_{i,j}\ \ \mathbf{x}_{p,q}\ }$
Cosine similarity to global mean	$F_{i,j} = \frac{\langle \mathbf{x}_{i,j}, \boldsymbol{\mu} \rangle}{\ \mathbf{x}_{i,j}\ \ \boldsymbol{\mu}\ }$

Table 14. **ImageNet-1K subset robustness**. Diffusion-classifier accuracy on 2K and 10K subsets with 95% Wilson confidence intervals.

Method	No accel.	ToMe (70%)	BiGain _{TM} (70%)	ToDo (2×)	BiGain _{TD} (2×)
Acc. ($n=2000$) (%) \uparrow	57.05 \pm 2.17	37.35 \pm 2.13	44.50 \pm 2.19	55.75 \pm 2.17	56.30 \pm 2.17
Acc. ($n=10000$) (%) \uparrow	57.92 \pm 0.97	39.85 \pm 0.96	45.25 \pm 0.98	56.50 \pm 0.97	57.59 \pm 0.97

Algorithm 3 Adaptive Block Merge (ABM): Fast BiGain_{TM} Variant

Require: Tokens $\mathbf{X} \in \mathbb{R}^{N \times d}$, block size b , merge ratio $r \in [0, 1]$, scorer \mathcal{F}

- 1: **function** ADAPTIVEBLOCKMERGE($\mathbf{X}, b, r, \mathcal{F}$)
- 2: $\mathbf{f} \leftarrow \mathcal{F}(\mathbf{X})$ \triangleright Compute frequency scores
- 3: $\mathcal{B} \leftarrow \text{BlockPartition}(\mathbf{X}, b)$ \triangleright Partition into $b \times b$ blocks
- 4: $\mathcal{B}_{\text{smooth}} \leftarrow \text{SelectLowestFreq}(\mathcal{B}, \mathbf{f}, r)$ \triangleright Select lowest r fraction blocks
- 5: $\mathbf{X}^{\text{merged}} \leftarrow \text{MergeBlocks}(\mathbf{X}, \mathcal{B}_{\text{smooth}})$ \triangleright Average selected blocks
- 6: $\mathbf{Z} \leftarrow \text{Process}(\mathbf{X}^{\text{merged}})$ \triangleright Apply attention
- 7: **return** RestoreBlocks($\mathbf{Z}, \mathcal{B}_{\text{smooth}}$) \triangleright Restore dimensions
- 8: **end function**

C.5. Additional Ablations and Results

We provide four targeted supplementary studies to further clarify the robustness and scope of our results: (i) robustness to the ImageNet-1K evaluation subset size, (ii) sensitivity of IE-KVD to α and its timestep schedule, (iii) compatibility between the merging and downsampling modules, and (iv) actual wall-clock speedups. Throughout this subsection, BiGain_{TM} refers to the merging module (L-GTM),

Algorithm 4 BiGain_{TD}: Interpolate-Extrapolate KV-Downsampling (IE-KVD)

Require: Tokens $\mathbf{X} \in \mathbb{R}^{N \times d}$, downsample factor s , interpolation-extrapolation factor $\alpha \in \mathbb{R}$

- 1: **function** BIGAINDOWNSAMPLE(\mathbf{X}, s, α)
- 2: $\mathbf{Q} \leftarrow \mathbf{X} \mathbf{W}_Q$ \triangleright Queries at full resolution
- 3: $\mathbf{K} \leftarrow \mathbf{X} \mathbf{W}_K, \quad \mathbf{V} \leftarrow \mathbf{X} \mathbf{W}_V$ \triangleright Keys and values
- 4: $\tilde{\mathbf{K}} \leftarrow \text{Interpolate/ExtrapolateDownsample}(\mathbf{K}, s, \alpha)$
- 5: $\tilde{\mathbf{V}} \leftarrow \text{Interpolate/ExtrapolateDownsample}(\mathbf{V}, s, \alpha)$
- 6: $\mathbf{Z} \leftarrow \text{Attention}(\mathbf{Q}, \tilde{\mathbf{K}}, \tilde{\mathbf{V}})$
- 7: **return** \mathbf{Z} \triangleright Output remains at full resolution
- 8: **end function**

while BiGain_{TD} refers to the KV-downsampling module (IE-KVD). Unless otherwise stated, we follow the same evaluation protocol as in the main paper. For SD-2.0, we report diffusion-classifier Top-1 accuracy (Acc@1, %) and generation quality (FID). For merging-based methods, the merge ratio is denoted by r ; for downsampling-based methods, the downsampling factor is denoted by s . For IE-KVD, α controls interpolation/extrapolation in KV downsampling; for generation we also consider linear schedules ($\alpha_{\text{start}} \rightarrow \alpha_{\text{end}}$). Wall-clock times are measured on a single RTX 4090 with FP16 and batch size 4 over 50 denoising steps, we report the U-Net step time averaged over 50 runs (VAE excluded).

Table 15. **IE-KVD α sensitivity.** SD-2.0 / Oxford-IIIT Pets diffusion classification accuracy (Acc., %).

α	0.0	0.5	0.8	0.9 (BiGain_{TD})	1.0	1.2
Acc. ($s=2$) (%) \uparrow	77.02	78.74	79.97	81.52	81.30	64.27
Acc. ($s=4$) (%) \uparrow	71.26	75.63	77.48	78.03	77.46	45.46

Table 16. **IE-KVD schedule ablation.** SD-2.0 / Oxford-IIIT Pets generation quality (FID \downarrow) under different linear schedules.

Linear schedule ($\alpha_{\text{start}} \rightarrow \alpha_{\text{end}}$)	FID \downarrow
ToDo	33.52
IE-KVD: 0.2 \rightarrow 0.8	35.56
IE-KVD: 0.5 \rightarrow 1.0	33.95
IE-KVD: 0.7 \rightarrow 1.0	33.89
IE-KVD: 0.8 \rightarrow 1.2	32.19
IE-KVD: 0.0 \rightarrow 1.2	32.54

Robustness to evaluation subset size. Table 14 addresses the concern that the ImageNet-1K classification results in the main paper are evaluated on a 2K subset for efficiency. We therefore expand the evaluation to 10K images in Table 14 and find that the relative ranking of methods remains unchanged, leading to the same qualitative conclusion. This indicates that the main findings are robust and not an artifact of the smaller subset.

Sensitivity of IE-KVD hyperparameters. Tables 15 and 16 examine the two main IE-KVD design choices: the interpolation–extrapolation parameter α and its timestep schedule. Accuracy is strongest around $\alpha \in [0.8, 1.0]$, showing that the default choice $\alpha = 0.9$ is not fragile, while overly aggressive extrapolation ($\alpha = 1.2$) degrades performance. For generation, FID varies only modestly across linear schedules, suggesting that IE-KVD is reasonably robust to the exact schedule.

Joint use of merging and downsampling. Table 17 studies two hybrid placements: L-GTM in the encoder with IE-KVD in the decoder, and the reverse. Both combinations remain stable for classification and generation, but neither exceeds the best single-module setting. This suggests that the two operators are compatible, although their gains are not simply additive.

Measured runtime. Finally, Table 18 reports actual UNet step time in addition to FLOPs. This complements Table 11, which focuses on merging-based batch-time measurements, by providing a unified runtime comparison that also includes downsampling and hybrid settings. The empirical speedups follow the same trend as the FLOP reductions, confirming that the proposed operators translate into real inference-time gains.

Table 17. **Joint use of L-GTM and IE-KVD.** SD-2.0 / Oxford-IIIT Pets with $r=0.7$, $s=2$, $\alpha=0.9$.

Method	Acc@1 \uparrow (%)	FID \downarrow
No accel.	81.03	35.01
ToMe	65.76	38.35
ToDo	81.30	33.52
BiGain _{TM}	74.63	37.73
BiGain _{TD}	81.52	32.19
L-GTM(enc) + IE-KVD(dec)	79.53	34.84
IE-KVD(enc) + L-GTM(dec)	79.23	36.90

Table 18. **Wall-clock UNet step time.** SD-2.0 on RTX 4090 (FP16, batch=4, 50 steps; averaged over 50 runs; VAE excluded).

Method	Time \downarrow (ms/step)	Speedup \uparrow (\times)	FLOPs \downarrow (G)
No accel.	235.65	1.00	804.26
ToMe	144.31	1.63	704.87
ToDo	145.50	1.62	717.44
BiGain _{TM}	142.88	1.65	704.99
BiGain _{TD}	150.30	1.57	717.44
L-GTM(enc) + IE-KVD(dec)	147.43	1.60	716.23
IE-KVD(enc) + L-GTM(dec)	146.39	1.61	712.49

D. Use of Large Language Models

We used an LLM to help solely polish the writing of the paper, while all ideas and experiments are conceived and carried out entirely by the authors.